A Comparison of Seeded and Nonseeded Orographic Cloud Simulations with an Explicit Cloud Model

MICHAEL P. MEYERS, PAUL J. DEMOTT, AND WILLIAM R. COTTON

Department of Atmospheric Science, Colorado State University, Fort Collins, Colorado

(Manuscript received 21 December 1993, in final form 14 September 1994)

ABSTRACT

Ice initiation by specific cloud seeding aerosols, quantified in laboratory studies, has been formulated for use in mesoscale numerical cloud models. This detailed approach, which explicitly represents artificial ice nuclei activation, is unique for mesoscale simulations of cloud seeding. This new scheme was applied in the simulation of an orographic precipitation event seeded with the specific aerosols on 18 December 1986 from the Sierra Cooperative Pilot Project using the Regional Atmospheric Modeling System (RAMS). Total ice concentrations formed following seeding agreed well with observations. RAMS's three-dimensional results showed that the new seeding parameterization impacted the microphysical fields producing increased pristine ice crystal, aggregate, and graupel mass downstream of the seeded regions. Pristine ice concentration also increased as much as an order of magnitude in some locations due to seeding. Precipitation augmentation due to the seeding was 0.1–0.7 mm, similar to values inferred from the observations. Simulated precipitation enhancement occurred due to increased precipitation efficiency since no large precipitation deficits occurred in the simulation. These maxima were collocated with regions of supercooled liquid water where nucleation by man-made ice nucleus aerosols was optimized.

1. Introduction

Precipitation processes in cloud systems in the Sierra Nevada have been investigated for many years because of their importance to the water resources of the area. The emphasis of these programs, such as the Sierra Cooperative Pilot Project (SCPP) (Reynolds and Dennis 1986), is to examine and quantify the microphysical and dynamical properties of these orographic cloud systems and to determine if weather modification is a viable alternative for enhancing precipitation in these areas.

This study applied an artificial ice formation parameterization specific to the ice nucleating aerosols used during a portion of the SCPP program for use in a detailed cloud model. The nucleation processes responsible for ice formation were quantified based on detailed laboratory studies performed at Colorado State University (CSU). A preliminary seeding simulation that employed a microphysical parcel model was used to demonstrate the details of ice formation implemented for artificial ice nucleus aerosols into the mesoscale model and to investigate expected dominant ice formation modes. The artificial nucleation parameterization was then added to the Regional Atmospheric Modeling System (RAMS) developed at CSU, which was used to examine the 18 December 1986 seeded orographic cloud system from SCPP. The World Meteorological Organization's (WMO) Third International Cloud Modeling Workshop (WMO 1994) provided the motivation for examining this case study. Three-dimensional (3D) nested-grid simulations were employed to fully evaluate the microphysical evolution of clouds in both seeded and nonseeded numerical studies and allowed comparison to the observed structure of the clouds.

2. Background

a. Historical

Numerical cloud models have been used by a number of researchers to simulate the effects of various seeding techniques in different types of clouds. Although one must treat the transfer of laboratory results into numerical models with some caution, DeMott (1994) has summarized evidence from atmospheric seeding tests that the laboratory results on ice initiation processes do correlate with observed cloud microphysical effects in many circumstances. The schemes employed by various researchers to initialize ice formation by man-made ice nucleus aerosols have varied widely. In some cases these schemes have been based on a combination of theory and laboratory results that are not necessarily compatible. Also, due to the lack of information, the schemes are seldom specific to the nucleant used in a particular operational or research

Corresponding author address: Dr. Michael P. Meyers, Department of Atmospheric Science, Colorado State University, Fort Collins, CO 80523.

© 1995 American Meteorological Society

program. A common scheme (e.g., Plooster and Fukuta 1975) has been to use the laboratory-measured ice nucleus effectiveness spectra (ice crystals per gram released), if available, to specify the number of ice crystals formed, with no regard to mechanism or a consideration of the potential time required for nucleation. This represents the simplest scheme for use in mesoscale models. Other researchers have sought to increase the complexity of implementing ice initiation. Young (1974b) included two mechanisms, deposition and contact nucleation (via Brownian and phoretic transport processes), in a detailed microphysical cloud model. Only contact-freezing nucleation was used in published nonspecific seeding simulations (Young 1974a), and the nucleus activity spectrum employed was not representative of most that have been measured for field generators. Hsie et al. (1980) simulated both contact-freezing and deposition nucleation in a study of seeding effects in continental cumulus clouds using a 2D time-dependent model. The nucleation mechanisms were applied to the laboratory measured effectiveness spectra of a nucleus for which the ice formation mechanisms were not known. The relative contribution to ice crystal formation by each mechanism was based on the theoretical work of Cooper (1974), which has not been directly verified. None of the above-mentioned models explicitly included condensation-freezing nucleation.

The nature of ice-nucleation mechanisms, rates, and activities can directly and indirectly influence the nature of numerical cloud model predictions of seeding effects. Orville et al. (1984) found unexpected dynamic effects in AgI seeding simulations of stratus clouds. This clearly related to the presumed nucleation activity and rates of ice crystal formation (instantaneous). Orville et al. noted the potential inadequacy of the nucleation scheme employed and its importance in the realization of quantitative results. Blumenstein et al. (1987) developed time- and temperature-dependent empirical expressions from experimental data obtained in the CSU isothermal cloud chamber and applied these in Rauber's (1981) 2D orographic cloud model. Her laboratory study demonstrated a slow (up to 100 min for completion) condensation-freezing nucleation process by AgI–NaI aerosols at near water saturation and a fast (within seconds) process when unspecified water supersaturations were induced. Also, nucleation activity increased in the supersaturated case. Assumptions of either the slow or fast nucleation process in Blumenstein's simulations yielded large differences in the amount and targeting of seeded snowfall. Lacking from this study was a more detailed knowledge of the exact response of the aerosols to differing magnitudes of supersaturation.

The numerical study presented in this paper takes advantage of the recent laboratory study of a particular ice nucleus aerosol that was used in a well-documented cloud seeding case study. It was sought to implement the high level of detail of ice nucleus response to varied temperature, humidity, and cloud conditions obtained in the laboratory study into mesoscale simulations. The goal was to have the capability to predict both the precipitation effects and observable cloud microphysical effects of seeding for comparison to observations.

b. Case study

The case selected for the modeling study was the 18 December 1986 SCPP case study that has been examined by Deshler et al. (1990). The day was characterized by a weak split-front, where the upper-level cold surge crossed Sheridan, California, (located at the base of the Sierra foothills) at 1500 UTC preceding a surface cold front that crossed Sheridan between 1800 and 2100 UTC. This environment has been noted to be favorable for the local production of supercooled liquid water (SLW) (Reynolds and Kuciauskas 1988), and consequently, three experiments were conducted between 1800 and 2000 UTC. Seeding was conducted in the SLW region at approximately −6°C in three 37-km seedlines. Most of the natural precipitation was orographically produced with peak precipitation rates observed at Kingvale, California, to be 1–1.5 mm h^{-1}. Deshler et al. (1990) inferred a precipitation seeding signature of 0.1–0.5 mm.

A range of hydrometeor species were observed during this case study including pristine ice crystals, rimed particles, aggregate snowfall, and rain. Figure 1, based on results reported by Deshler et al. (1990), depicts an idealized x–z section of the measured distribution of ice and liquid water species at 1730 UTC (before seeding). Large aggregates were observed over a wide region west of the Sierra crest at temperatures warmer than −10°C. Rimed crystals and graupel were noted in more localized regions further up the barrier at this time. Pristine ice crystals predominated at higher altitudes and directly over the mountain crest. Pristine ice crystal concentrations were observed to be less than 10 L^{-1} (mean values), with maximum values as high as 20–30 L^{-1} during natural conditions. Ice crystal concentrations over 100 L^{-1} (peak values) were observed in the seeded cloud.

The ice nucleus aerosols used for seeding were AgI–AgCl aerosols produced by combustion of acetone-based solutions of AgI (silver iodide), NH_4I (ammonium iodide), and NH_4ClO_4 (ammonium perchlorate). The generation of AgI–AgCl aerosols in this manner has been described by DeMott et al. (1983), who noted optimization of ice nucleation efficiency when NH_4ClO_4 was used at the 30 mol % level with respect to AgI. Except for the use of 3% AgI by weight instead of 2%, the solutions burned in SCPP aircraft-mounted generators during this case study were the same ones used by DeMott et al. (1983) and DeMott (1994) in laboratory studies. Potential differences in particle size distributions (PSDs) generated at th lab-

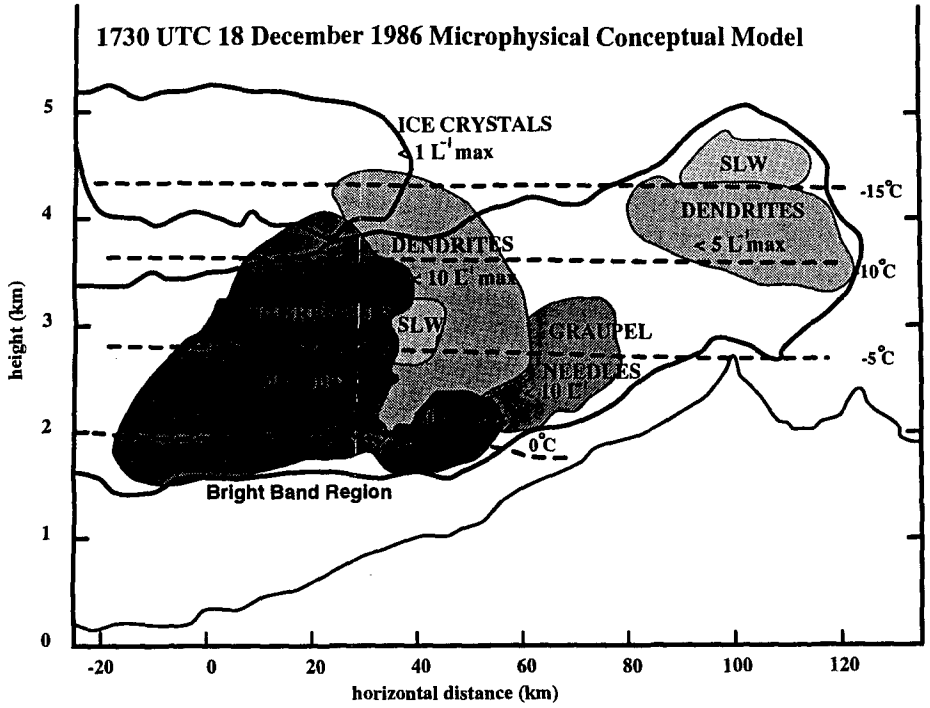

FIG. 1. Cross section of the microphysical structure over the barrier for 1730 UTC 18 December 1986 adapted from Deshler et al. (1990). Microphysical characteristics from aircraft measurements are highlighted by stippled areas. Cloud boundary and temperature structure is also included. Sheridan is located near the 0-km distance, and Kingvale is located near the 80-km distance.

oratory and in the field generators lead to some amount of uncertainty in specifying seeding for numerical calculations (DeMott 1991; Deshler and Reynolds 1991). This sensitivity was also examined in this paper.

3. Parameterization of artificial ice nucleation processes

a. Development of parameterization

An important goal of the study presented in this paper was to explicitly specify ice formation by the actual artificial ice nuclei (IN) used in the SCPP program for the simulation that follows in section 4c. This detailed approach has not previously been used for mesoscale simulations of case studies of clouds seeded for precipitation enhancement. Ice formation is quantified as a fraction of available IN (based on conservative mixing ratios of seeding material released in known quantities) determined for deposition, condensation-freezing, immersion-freezing, and contact-freezing nucleation processes based on the laboratory studies of DeMott (1990, 1994). Deposition nucleation is used to describe ice formation ascribed only to a response to ice supersaturation. Condensation freezing is the instantaneous ice nucleation response of aerosols to water supersaturation, while immersion freezing describes the freezing of cloud droplets containing previously scavenged (by condensation or collection) ice nucleus aerosols. Contact freezing describes the freezing that instantaneously follows collisions between ice nucleus aerosols and cloud droplets caused by various transport mechanisms that are not instantaneous. The experimental results represented in the equations presented by DeMott (1994) go far beyond the results of DeMott et al. (1983), which quantified primarily the contact-freezing activity of AgI–AgCl aerosols. Dependencies on temperature, humidity, and particle size were included as appropriate for each process.

For implementing explicit seeding into RAMS, the size dependence was first removed from the equations given by DeMott (1994) by integrating them over a particle size distribution considered to be representative of that produced operationally. Unfortunately, the size distribution of AgI–AgCl aerosols produced by the airborne solution-combustion generator used in the SCPP case study was not measured. Two possibilities were considered. DeMott et al. (1983) presented an AgI–AgCl size distribution characteristic of a ground-based solution-combustion generator. A size distribution more characteristic of airborne solution-combustion generators was also estimated for AgI–AgCl aerosols. This distribution was based on years of laboratory data collected for airborne generators burning in a wind tunnel flow simulating flight speeds at the CSU Cloud Simulation and Aerosol Laboratory. Both distributions

can be reasonably well approximated by the continuous gamma distributions as shown in Fig. 2. These gamma functions with shape parameter equal to 2 are of the form

$$f(D) = \frac{D}{D_n^2} \exp\left(-\frac{D}{D_n}\right), \quad (3.1)$$

where D is diameter and D_n is the scaling diameter. It was determined that $D_n = 2.7 \times 10^{-6}$ cm provides an excellent fit for the AgI–AgCl PSD from DeMott et al. (1983), while $D_n = 1.5 \times 10^{-6}$ is probably more characteristic of an aircraft generator PSD.

The composite aircraft generator PSD was selected for the mesoscale model simulations as the most likely AgI–AgCl size distribution present following seeding on 18 December 1986. The consequence on ice formation compared to the use of the published ground generator PSD is demonstrated through the use of microphysical parcel model simulations later in this section. In integrating DeMott's equations over the selected PSD, environmental dependencies on temperature, ice supersaturation, and water supersaturation were retained, and the results for each ice formation mechanism were fit to a computationally efficient polynomial.

The total aerosol fraction nucleating ice by deposition F_{dep} was found to be

$$F_{dep} = a(S_i - 1) + b\left(\frac{273.16 - T}{T_0}\right) + c(S_i - 1)^2 + d\left(\frac{273.16 - T}{T_0}\right)^2 + e(S_i - 1)^3, \quad (3.2)$$

with constants $T_0 = 10.0$ K, $a = -3.25 \times 10^{-3}$, $b = 5.39 \times 10^{-5}$, $c = 4.35 \times 10^{-2}$, $d = 1.55 \times 10^{-4}$, and $e = -0.07$. Here S_i is the ice saturation ratio, T is in kelvins, and this equation was taken to be valid when $S_i > 1.04$ and $T <= 268.2$ K. The total aerosol fraction nucleating ice by condensation freezing F_{cdf} was parameterized as

$$F_{cdf} = a\left(\frac{268.66 - T}{T_0}\right)^3 (S_w - 1)^2, \quad (3.3)$$

with constants $T_0 = 10.0$ K, $a = 900.0$. This result was taken to be valid when $T < 268.66$ K and water saturation ratio $S_w > 1.0$. In a similar way, for the immersion-freezing nucleation fraction F_{imf}, it was found that

$$F_{imf} = a(F_{imm})\left(\frac{268.2 - T}{T_0}\right)^b, \quad (3.4)$$

with $T_0 = 10.0$ K, $a = 0.0274$, and $b = 3.3$, valid for $T < 268.2$ K. The use of this equation, however, also requires the knowledge of the fraction of nonactivated aerosol immersed in drops at any time and location (F_{imm}). This would be difficult to follow explicitly in a mesoscale model with bulk microphysics. Fortunately, the analysis of the relative contributions of the different ice formation mechanisms for AgI–AgCl aerosols made later in this section justified the omission of immersion-freezing nucleation from the mesoscale seeding simulation. The equation is presented here for the sake of completeness.

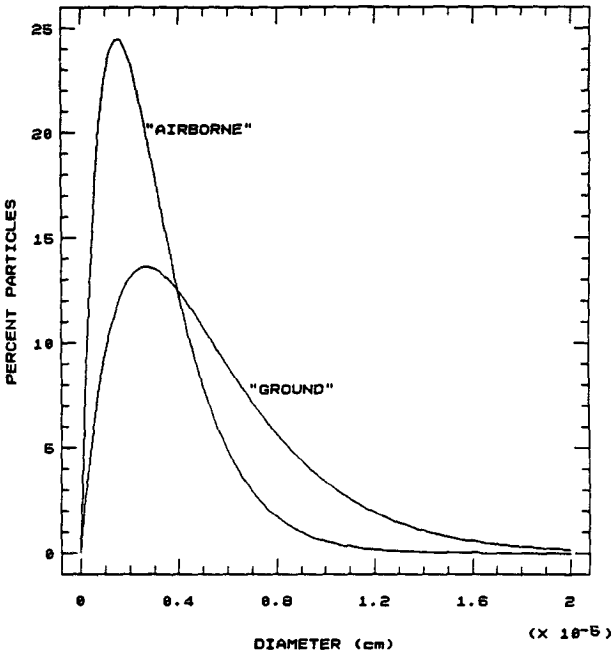

FIG. 2. Particle size distributions for airborne and ground-based measurements.

For contact-freezing nucleation, a parameterization was sought that would be compatible with the way that cloud water and scavenging of aerosols by cloud water are treated in RAMS. Namely, cloud droplet number concentration is fixed, cloud droplet diameter is allowed to vary, and aerosol size is fixed at one value. The geometric mean diameter of the artificial ice nuclei was taken as 2×10^{-6} cm for use in calculating collection rates by cloud droplets in RAMS. Rather than using the activity of this average size, the fraction of the total AgI–AgCl aerosol population potentially active as contact-freezing nuclei (F_{ctf}) was estimated by integrating the size-dependent equation given by DeMott (1994) over the selected size distribution. This gave

$$F_{ctf} = F_{scav}[a + b(S_i - 1) + c(S_i - 1)^2 + d(S_i - 1)^3 + e(S_i - 1)^4 + f(S_i - 1)^5 + g(S_i - 1)^6], \quad (3.5)$$

where the constants are given by $a = 0.0878$, $b = -3.7947$, $c = 52.3167$, $d = -255.4484$, $e = 568.3257$, $f = -460.4234$, and $g = -63.1248$. The term F_{scav} is the fraction of the total aerosol population scavenged by cloud droplets in a given grid volume in one time

step. Calculation of F_{scav} follows Young (1974a) for the parcel model simulations. It thus depends in time on the net collection kernel for Brownian, phoretic, and aerodynamic transport of aerosol to cloud droplets. Calculation of F_{scav} in RAMS follows the simplification of Young's equations given by Cotton et al. (1986). This equation was taken to be valid for $S_i > 1.058$ and for $T < 269.2$ K.

For all of the equations, extension below about 253 K implies extrapolation from experimental results, although values appear physically reasonable to as low as 248 K. In all cases as well, F is not allowed to exceed a maximum of 1.0. Extraordinary circumstances would be required to achieve such a result.

b. Initialization of seeded aerosol concentrations

For initializing seeded aerosol mass and concentration in the numerical simulations, the published aerosol mass release rates, aircraft speed, and horizontal and vertical dispersion rates were combined with the numbers of particles per gram released based on the PSD to determine the initial seeded volume aerosol concentration. This volume concentration was determined at a time of 6 min after seeding was initiated. At this time, about two-thirds of a 37-km seeding line had been dispensed, and the initial plume would have filled more than 10% of a 1000-m horizontal and 100-m vertical grid box used in the 3D numerical simulations with RAMS. In the seeding simulation, the entire grid was filled with the nuclei concentration thus determined. Therefore, the cloud was overseeded by several times from a total mass standpoint. This method was considered to be a reasonable compromise to overcome the current inability to accurately represent dispersion of seeded mass and concentrations at subgrid scales in mesoscale models. To accurately predict plume concentrations in the model immediately after seeding would have required excessively overseeding a model grid volume and thus greatly overestimating seeding effects on cloud microphysics and precipitation. Conversely, assuming the initial concentrations to be equivalent to those present at the time after the grid volumes were filled (30–40 min) would have greatly underestimated subsequent plume concentrations and missed much of the ice formation occurring by contact-freezing nucleation after the onset of seeding.

The published ice nucleus aerosol mass generation rate was 0.4 g km^{-1}. The speed of the cloud seeding aircraft was 80 m s^{-1}. Horizontal and vertical dispersion rates were estimated as 1.0 and 0.1 m s^{-1}, respectively. Integrating the PSDs shown in Fig. 2 gives 1×10^{15} and 4×10^{15} particles per gram nucleant generated, respectively, for the "ground" and "airborne" cases. Using all of the above values, initial seeded concentrations at 6 min after release were determined as 40 000 and 160 000 L^{-1}, respectively, for the "ground" and "airborne" PSDs. The latter result was used for RAMS simulations.

c. Parameterization tests

Preliminary to the mesoscale model simulations, some simulations were done with a microphysical parcel model. The purposes of this exercise were to investigate the importance of knowledge of the artificially generated aerosol size distribution, to demonstrate the validity of the ice nucleation parameterizations, and to determine the expected relative importance of the different ice formation processes for conditions relevant to the 18 December 1986 case study. The parcel model used was a modified version of the model described by Rokicki and Young (1978); a derivative of the 2D microphysical model described in detail by Young (1974b). The version employed is very nearly the same as used and described by Stith et al. (1994), Rogers et al. (1994), and DeMott (1994) for various investigations of ice initiation due to natural and man-made aerosols. In broad terms, the model simulates the three major processes of nucleation, diffusion, and collection that are key to precipitation formation. Precipitation does not occur from the parcel, and, except for a specification of vertical motion, cloud dynamics is not considered.

For the parcel model simulations, artificial ice initiation by deposition, condensation-freezing, contact-freezing, and immersion-freezing nucleation followed either the detailed results as a function of AgI–AgCl particle size summarized by DeMott (1994) or the parameterizations given in Eqs. (3.2)–(3.5). The F_{scav} realized in any time step was determined by the collection rates of ice nuclei by cloud droplets due to the combined effects of Brownian collection, thermophoresis, diffusiophoresis, and aerodynamic capture. Calculations of collection rates followed the equations from Young (1974a) and the specification of the particle size distribution. Freezing occurred at the droplet temperature that is explicitly calculated in the model.

In the simulations presented, a constant updraft was imposed on a seeded cloud parcel since we were only interested in demonstrating results to be expected in the mesoscale simulations. A representative 0.2 m s^{-1} updraft was chosen for a parcel initialized 0.5% supersaturated with respect to water at −6.3°C and 700 mb. CCN coefficients were adjusted to cause 130 cm^{-3} droplets to form initially, consistent with observations. Fifteen discrete size bins were used to specify each of the two different particle size distributions used.

Figure 3 shows parcel thermodynamic and microphysical evolution with time, as well as the cumulative production of ice crystal concentrations by the four nucleation mechanisms quantified for three simulations. Two simulations demonstrate the effect of the presumed aerosol size distribution on ice formation in the parcel model. Dashed curves are for the presumed aircraft generator particle size distribution. The dash–dot curves presume the size distribution given by DeMott et al. (1983) for a ground-based generator.

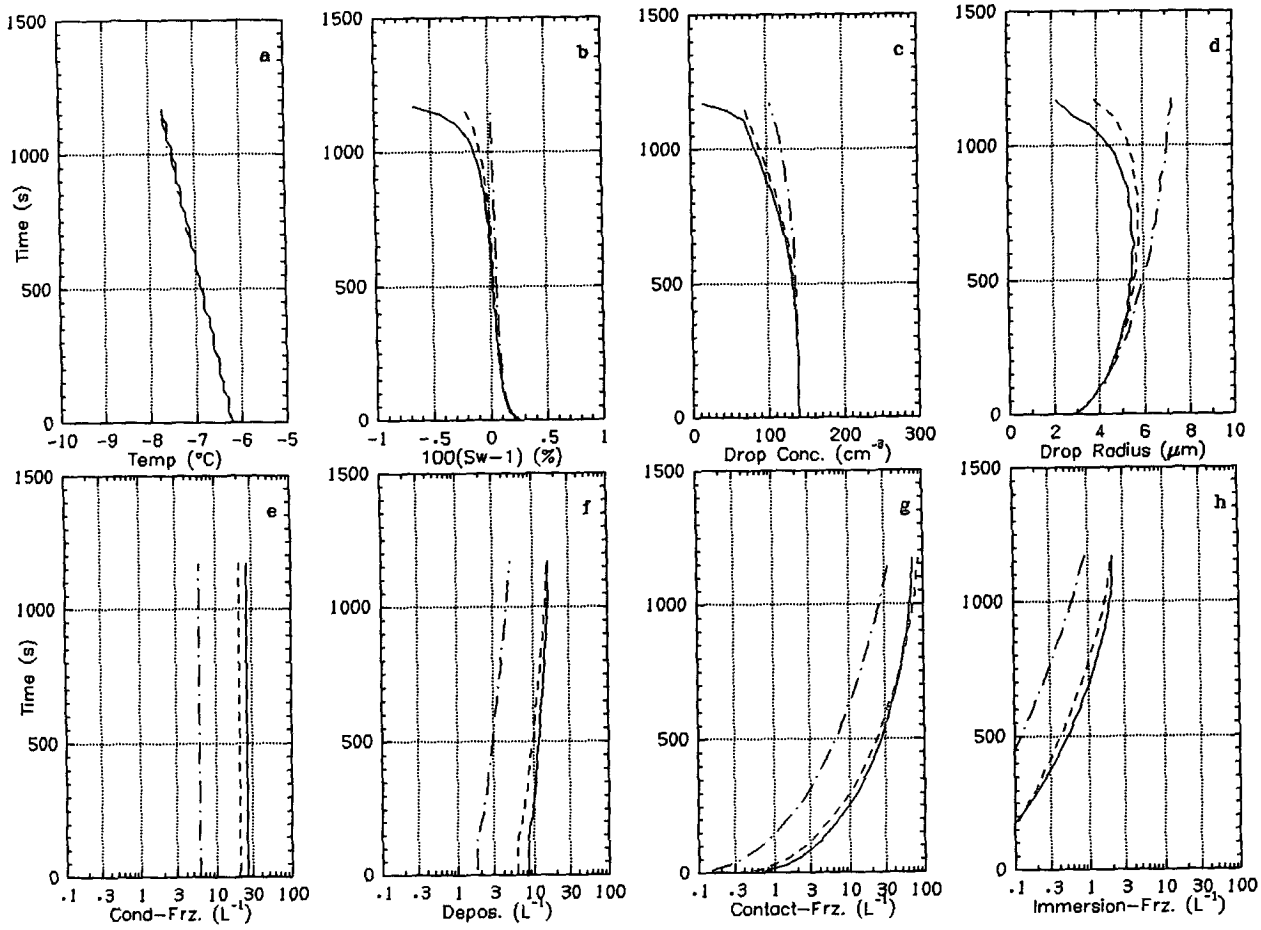

FIG. 3. Parcel model simulation temporal profiles of (a) temperature, (b) percent water supersaturation, (c) droplet concentration, (d) average droplet radius, and (e)–(h) cumulative ice crystal concentrations nucleated by different ice-formation modes. Dashed curves are for the presumed aircraft generator particle size distribution. The dash–dot curves presume the size distribution given by DeMott et al. (1983) for a ground-based generator. The solid curves are from the parameterized equations (aircraft generator PSD).

The detailed equations from DeMott (1994) were used in these simulations. It is seen that the size distribution can be quite important to the realized effect of seeding on ice crystal concentrations. A factor of 3 decrease in concentrations was noted when the size distribution measured from a ground generator was used instead of the typical airborne generator distribution. The somewhat lower ice nucleus activity of the smaller aerosols produced by aircraft units was more than compensated for by the increased numbers of smaller particles. The airborne generator size distribution was deemed most appropriate for use in the mesoscale simulation. Figure 3 also demonstrates the excellent performance of the parameterized descriptions of ice-formation processes. The simulation results using the parameterized equations developed for use in the mesoscale model are indicated by the solid curves in Fig. 3. These results are directly comparable to the dashed curves (detailed equations, aircraft generator PSD). Only a very slight tendency for the parameterization to overestimate ice formation was found.

Figure 3 also demonstrates that the initial concentrations of ice nucleated when AgI–AgCl aerosols are released directly into a wintertime orographic cloud will come primarily from deposition and condensation-freezing events and will therefore strongly depend on the ambient humidity or any higher supersaturation potentially generated during combustion (Finnegan and Pitter 1988). For the initial conditions specified, deposition and condensation freezing contribute nearly 30 L^{-1}, representing approximately 0.02% of the total aerosol almost instantly for the aircraft generator PSD. Condensation freezing was less important at later times despite the decrease in temperature because water supersaturation decreased to near zero. Deposition continued to generate significant numbers of ice crystals as the temperature decreased and ice supersaturation increased. Contact freezing was predicted to be a minor player for the first several minutes after seeding because collection rates are slow in the orographic cloud and nucleation efficiencies are lower at warmer temperatures. This mechanism began to dominate ice forma-

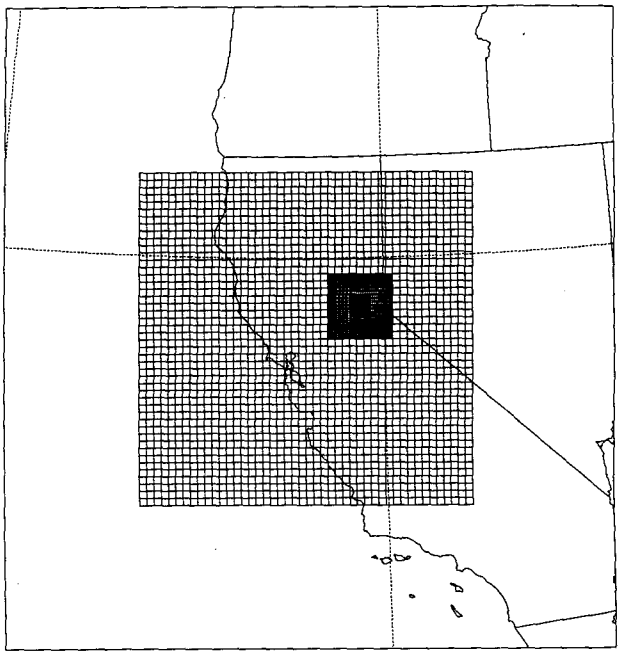

FIG. 4. Grid configuration of 3D nested-grid model. Grid 1 is the largest hatched grid ($\Delta x = \Delta y = 16$ km), with grid 2 being the next largest hatched region ($\Delta x = \Delta y = 4$ km), and grid 3 being the dark shaded region ($\Delta x = \Delta y = 1$ km).

tion more as parcel temperature lowered. This effect would have been greatly reduced if horizontal dispersion was considered in the simulation as it was in the RAMS simulations presented in the next section. Immersion freezing is an insignificant contributor to ice formation for the conditions simulated. Considering this factor and the high overhead of implementing such a process in larger-scale simulations, it was omitted as a potential ice formation process in the mesoscale simulations.

While the parcel model simulations cannot adequately simulate the seeding situation, they do indicate that the concentrations of ice crystals formed based on laboratory results are in line with those inferred to have formed from seeding (Deshler et al. 1990). Namely, the ice crystal concentrations in the seeded plume are predicted to be between 10 to more than 100 L^{-1}.

4. Mesoscale model simulations

Mesoscale model simulations were done using a three-dimensional version of RAMS. Preliminary 2D sensitivity tests (not shown) demonstrated the importance of releasing the seeding material in the correct location to optimize artificial nucleation processes. One problem found with the 2D simulations was that the SLW was very transient and the resultant precipitation was increased only when the seeded material was released in a region of SLW. Use of the 3D version of the model allowed for a more realistic depiction of the spatial variability of the liquid water. These three-dimensional simulations also allowed a variable initialization that alleviates some of the problems inherent to horizontally homogeneous initializations.

a. Model description

The numerical model used in this study was a version of the RAMS cloud model developed at CSU (Tripoli and Cotton 1982, 1989; Cotton et al. 1982, 1986). RAMS was configured using the nonhydrostatic, fully compressible momentum equations; a thermodynamic energy equation; and equations for liquid- and ice-phase precipitation processes. The predicted variables included the three velocity components; the Exner function π; the ice–liquid water potential temperature θ_{il} (Tripoli and Cotton 1981); pristine ice crystal concentrations; and mixing ratio of total water, rain, pristine ice crystals, graupel particles, and aggregates (Cotton et al. 1986). Note that pristine ice crystals in the Cotton et al. (1986) parameterization represents freshly nucleated, vapor-grown ice crystals. Ice crystals formed by seeding, while not being pristine in the purest sense, are placed in the pristine ice crystal category of the model. Potential temperature, temperature, cloud droplet mixing ratio, water vapor mixing ratio, and pressure are calculated diagnostically (Tripoli and Cotton 1982). Horizontal and vertical turbulence are parameterized using an eddy viscosity closure scheme, as described by Tripoli and Cotton (1982). The equations are integrated numerically by a time-splitting procedure for a nonhydrostatic, compressible system (Tripoli and Cotton 1982). A Klemp and Wilhelmson (1978) radiative-type lateral boundary condition was used. A terrain-following sigma-z vertical coordinate system was used following Gal-Chen and Sommerville (1975a,b). A comprehensive overview of the microphysics model was given in Flatau et al. (1989). Natural primary ice formation in RAMS followed from two models that quantify four ice formation mechanisms. The deposition/condensation-freezing model of Meyers et al. (1992) was used to describe nucleation from the vapor state below and above water saturation. This model is based on data from continuous flow diffusion chambers relevant to both deposition nucleation and the sorption form of condensation freezing. It is possible that this parameterization also accounts for the natural immersion freezing IN population. Ice crystal concentrations are specified as a function of ice supersaturation, which varies with temperature and vapor mixing ratio forecast by the model. Contact freezing was also quantified following Meyers et al. (1992). The total potential numbers of contact freezing nuclei effective per liter of air is based on a compilation of various laboratory data. The fraction of this potential activity realized in any time step is determined by the collection rates of ice nuclei by cloud droplets due to the combined effects of Brownian collection, thermo-

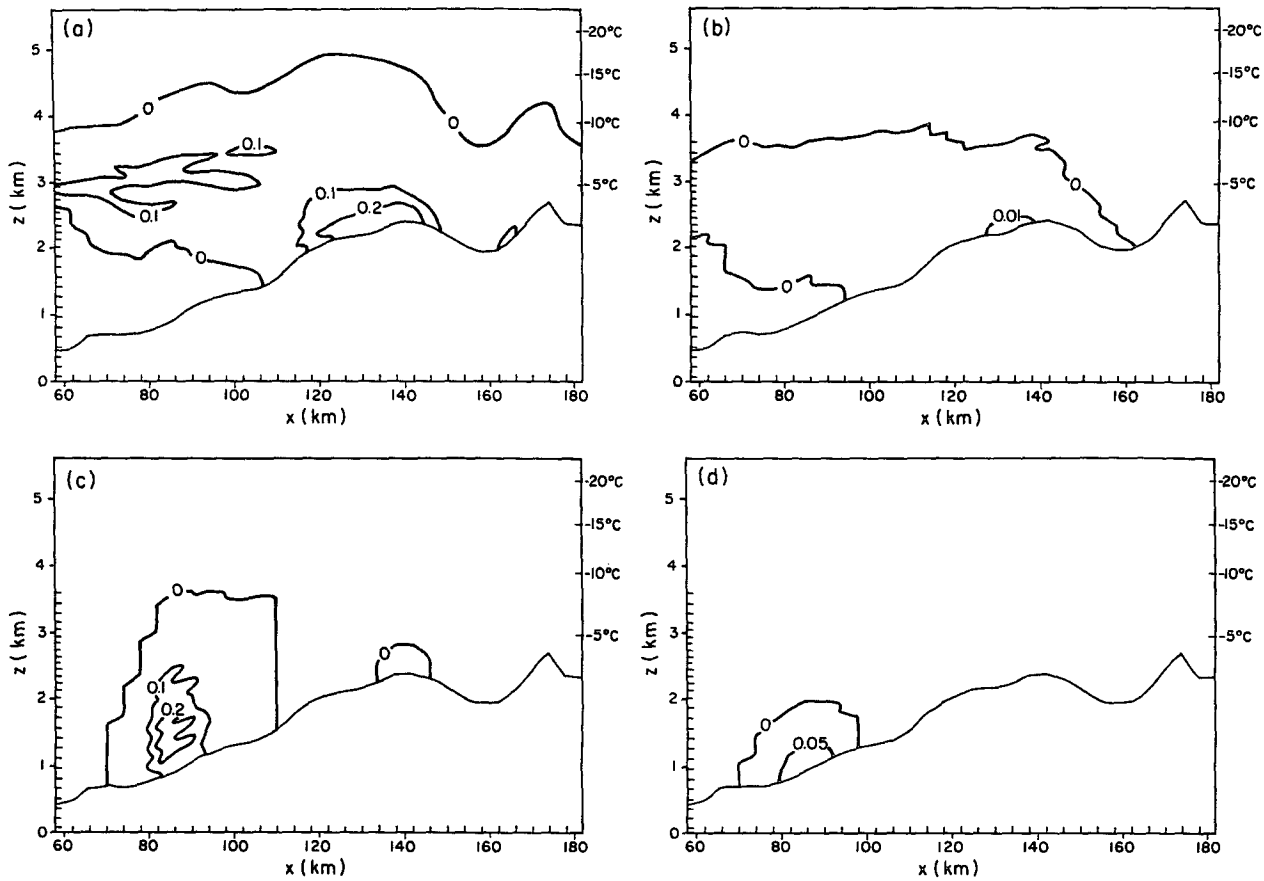

FIG. 5. (a) The simulated pristine ice mixing ratio on grid 2 [x–z cross section along the line of y = 28 of grid 2 (see Fig. 4)] at 1730 UTC (nonseeded case), contour interval is 0.1 g kg^{-1}. (b) The simulated aggregate mixing ratio on grid 2 at 1730 UTC, contour interval is 0.01 g kg^{-1}. (c) The simulated graupel mixing ratio on grid 2 at 1730 UTC, contour interval is 0.1 g kg^{-1}. (d) The simulated rain mixing ratio on grid 2 at 1730 UTC, contour interval is 0.05 g kg^{-1}. The abscissa is the x direction (km), the left ordinate is the z direction (km), and the right ordinate is temperatures (°C). The x and y labels on this and subsequent figures denote horizontal distance (km) from the center of the coarsest grid.

phoresis, and diffusiophoresis. In the version of RAMS used in this study, cloud droplet concentration was specified, and average diameter was diagnosed. Collection rates for contact freezing were computed based on average cloud droplet diameter and mean aerosol diameter following Cotton et al. (1986). The diameter of natural contact-freezing aerosols was assumed to be 1×10^{-5} cm. Secondary ice formation by the Hallett–Mossop mechanisms was quantified as described by Cotton et al. (1986).

Since cloud water was diagnosed in the mesoscale simulations, water supersaturation would always be zero. However, since artificial nucleation due to condensation freezing depends on water supersaturation, a diagnostic scheme was used to calculate water saturation. It was assumed that the supersaturation results from a balance between the dominant removal mechanism (the diffusional growth of cloud droplets and ice crystals) and the dominant production mechanism (the moist-adiabatic cooling due to vertical motion) (Cotton et al. 1986).

b. Model setup

The setup of the 3D nested-grid domain is shown in Fig. 4 and includes 48 × 38 × 48 grid points on the two coarsest grids (grid 1 and grid 2), with 50 × 50 × 49 on the fine grid (grid 3). The horizontal grid spacing is 16 km on grid 1, 4 km on grid 2, and 1 km on grid 3. The vertical grid spacing was stretched from 100 m in the seeded region to 800 m near model top. A 30-s topography dataset was used. A long time step of 30 s was used on the coarsest grid with a 5-s time step on the fine grid. An inhomogeneous initialization from NMC gridded data from 1200 UTC 18 December and 0000 UTC 19 December 1986 was used. Both the seeded and nonseeded simulations were run out to 2200 UTC and include full microphysics. The seeded run was restarted at 1900 UTC from the nonseeded simulation, at which time ice nucleus aerosols were introduced into the model. Only one release of ice nucleus aerosols was done in the seeded simulation, which is different from the 3 releases that occurred in the field

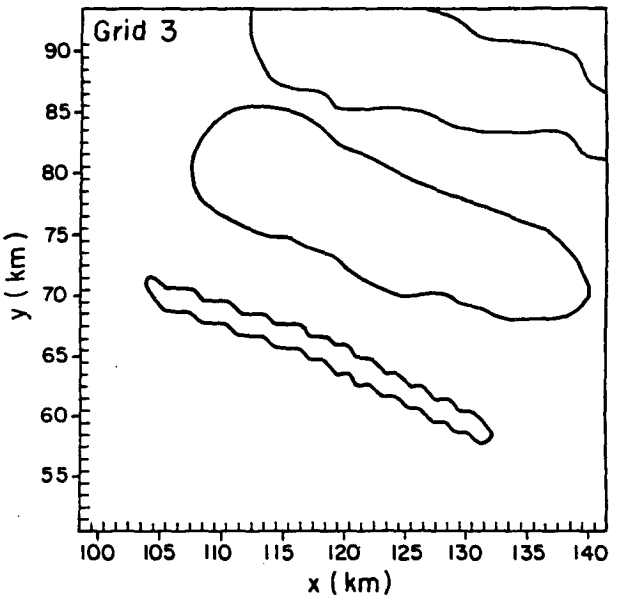

FIG. 6. The areal extent of the seedline as viewed from above (described in text) on grid 3 at t = 1900 UTC (at seeding), t = 1930 UTC (0.5 h after seeding), and at t = 2000 UTC (1.0 h after seeding).

experiment. Initialization of seeded aerosol concentrations was given in section 3b. The location of the simulated seedline was determined from the elevation and temperatures of the initial seedline (Deshler et al. 1990). The simulated seedline was nearly 37 km long and placed at the appropriate grid locations between the −6°C and −7°C isotherms.

c. *Model results*

It was important that the model simulated the natural precipitation processes properly before seeding was initiated. Figure 5 shows x–z cross sections of a few microphysical fields from the nonseeded simulation that can be compared to the observed structure shown in Fig. 1. The simulated pristine ice mixing ratio on grid 2 shows the ice cloud extending from 2 to 5 km MSL with peak amounts up to 0.2 g kg^{-1} (Fig. 5a). Predicted peak concentrations of pristine ice crystals are 10–25 L^{-1} (not shown), which were close to observed values of 10–30 L^{-1}. In Fig. 1 the observations showed an upper and lower cloud layer with precipitation occurring between the two layers at 4 km MSL. This feature would be quite difficult to predict in the model, however, since any precipitation falling out of the upper cloud would have appeared as one of the precipitating categories. Therefore the simulated structure predicted the pristine ice mixing cloud to extend from 2 to 5 km MSL. Aggregation was observed across most of the lower cloud but mostly confined below 3 km MSL with peak values near 0.07 g kg^{-1}. Simulated values of aggregate mixing ratio shown in Fig. 5b indicate that the aggregates were confined to below 3.5 km MSL, but peak values were 0.01 g kg^{-1}, which was less than the observed values. The graupel and rain mixing ratio fields are shown in Figs. 5c and 5d. These fields show melting precipitation below 1.5 km MSL in the form of graupel (partially melted pristine ice crystals are converted to graupel in the model) and rain occurring over the lower portion of the barrier. Peak values were 0.2 g kg^{-1} for graupel mixing ratio and 0.05 g kg^{-1} for rain mixing ratio. These simulated fields were close to the location of the higher reflectivities associated with an apparent bright band, resulting from melting ice particles, observed in this region (Fig. 1). Another area of graupel was predicted over the barrier crest. However, this region was located lower in elevation and was smaller in magnitude than observed.

After demonstrating the reasonableness of the simulation, the effects of releasing ice nucleus aerosols in the simulation can be examined. The initial seedline is shown in Fig. 6 at 1900 UTC. This figure depicts the areal extent of the artificial ice nuclei plume viewed from above at different times to show the relative advection and dispersion of the seeding material. The plume-edge concentration value was arbitrarily set to 10 L^{-1}. The relative advection speed of the plume in the simulation was 10 m s^{-1}, which was comparable to the advection speed of the plumes in the observations (10–15 m s^{-1}). By 2000 UTC the seed started to exit the northern border of grid 3.

The simulated pristine ice crystal concentrations from grid 3 at 3000 m MSL are shown in Fig. 7. This height was used since it was in proximity to the location of the seed release. At 1920 UTC, 20 min after the seed was introduced, the pristine ice crystal concentration field exhibited a similar structure as the seedline (Fig. 6), with a broad area of greater than 20 L^{-1}. Peak values were 120 L^{-1} (Fig. 7a), which is somewhat higher than the peak pristine ice crystal concentrations observed (greater than 100 L^{-1}). The location of the pristine ice crystal maxima was just downstream of a broad region of SLW seen in Fig. 8, which enhanced artificial ice nucleation. The overall structure of the pristine concentration field advected to the northeast by 1940 UTC (Fig. 7b), with a broad area of greater than 20 L^{-1}, a western peak of 60 L^{-1}, and an eastern peak of 110 L^{-1}. Peak concentrations decreased to 60 L^{-1} by 2000 UTC (Fig. 7c). Simulated pristine ice crystal concentration maxima from the nonseeded run during this period was 10 L^{-1} (Fig. 7d).

The effect of cloud seeding on other microphysical quantities was also quite significant. Figure 9 shows the predicted pristine ice mixing ratio fields from the seeded and nonseeded runs at 2000 UTC. In the seeded run the pristine ice mixing ratio field extended over a broader area than the nonseeded run, and peak values of the seeded run (0.35 g kg^{-1}) were nearly twice as much as the nonseeded run. There was more graupel mass (not shown) being produced in the seeded run

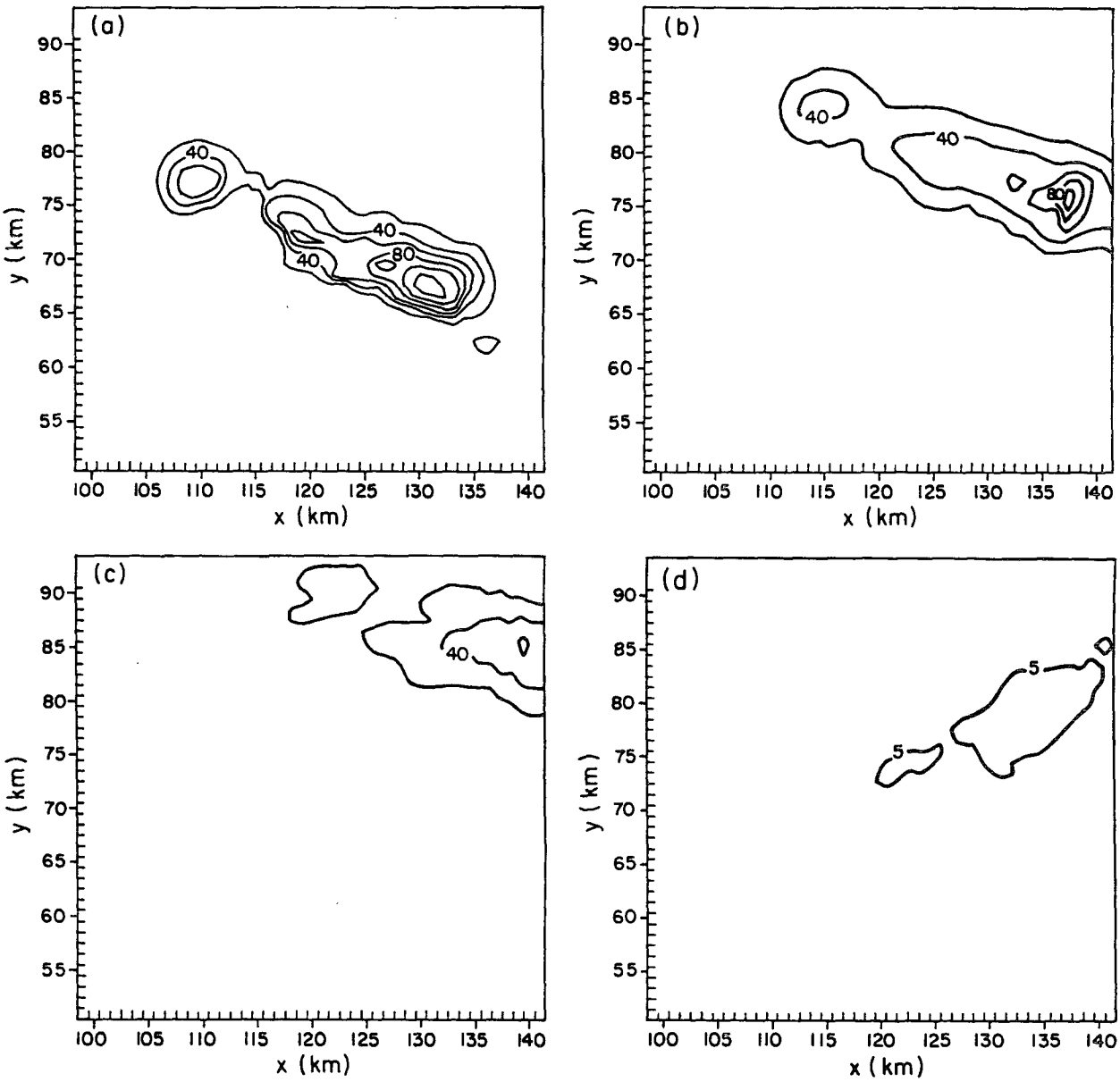

FIG. 7. The simulated pristine ice crystal concentrations for the seeded run at 3000 m MSL on grid 3 at (a) 1920, (b) 1940, and (c) 2000 UTC, with a contour interval of 20 L^{-1}. (d) Pristine ice crystal concentrations from the nonseeded run at 2000 UTC with a contour interval of 5 L^{-1}.

with peak values of 0.05 g kg^{-1}, more than double the values predicted in the nonseeded run. The aggregate mixing ratio maximum (not shown) was produced downstream of the pristine ice mixing ratio peak, with peak values in the seeded run of 0.02 g kg^{-1}. The nonseeded run produced negligible aggregation at this vertical level.

Since the exact location and times of the observed seed releases were different than the one seed release in the numerical experiment, spatial verification of the observed precipitation distribution was not considered. However, comparisons between the seeded and nonseeded precipitation distributions demonstrating the sensitivity of the seeding was examined. Figure 10 shows the precipitation difference between the seeded simulation and the nonseeded simulation by 2200 UTC. Differences in the precipitation amounts between the two runs showed that for this case, the increases due to the cloud seeding did not necessarily take precipitation from another location. Only one small area of minima occurred that had more precipitation in the nonseeded run than the seeded run. Simulated precip-

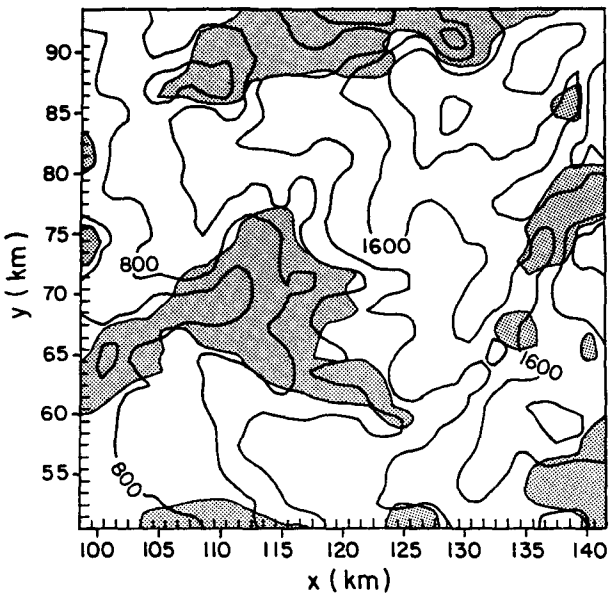

FIG. 8. The simulated cloud water mixing ratio on grid 3 at 1930 UTC at 3000 m MSL, values greater than 0.1 g kg^{-1} are stippled. Topography is also included with contour interval is 200 m.

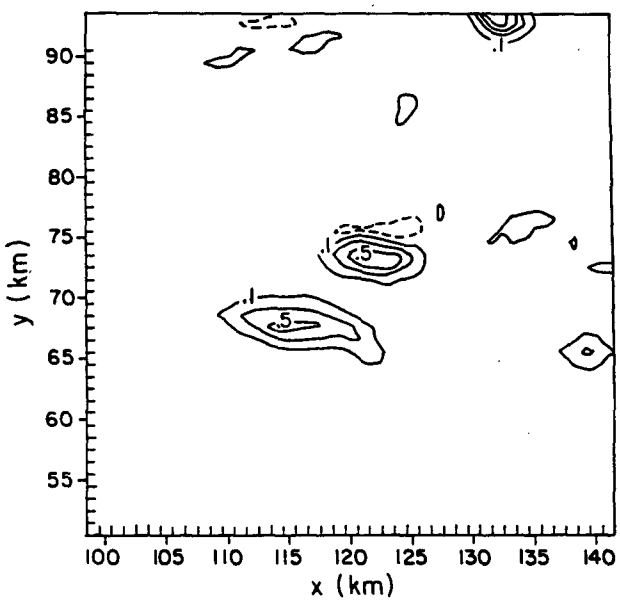

FIG. 10. The simulated precipitation difference between the seeded and the nonseeded runs for grid 3. Solid lines show seeded run greater, dashed lines show nonseeded run greater. Precipitation values range from −0.1 to 0.7 mm with an interval of 0.2 mm.

itation increases due to seeding were up to 0.7 mm, which compared quite reasonably with the inferred seeding signature of 0.1–0.5 mm. Each of the significant precipitation maxima from the seed simulation were located near regions of SLW shown in Fig. 9. These SLW regions, which may have been enhanced by topographic forcing, generated significant amounts of artificially produced pristine ice crystal mass that subsequently precipitated. The precipitation augmentation over the middle of the domain was located downstream of the initial seedline and occurred by 2000 UTC. The second precipitation region in the northeast portion of the domain was activated by another broad region of SLW, which enhanced precipitation efficiencies due to riming of the artificially produced ice particles. Overall,

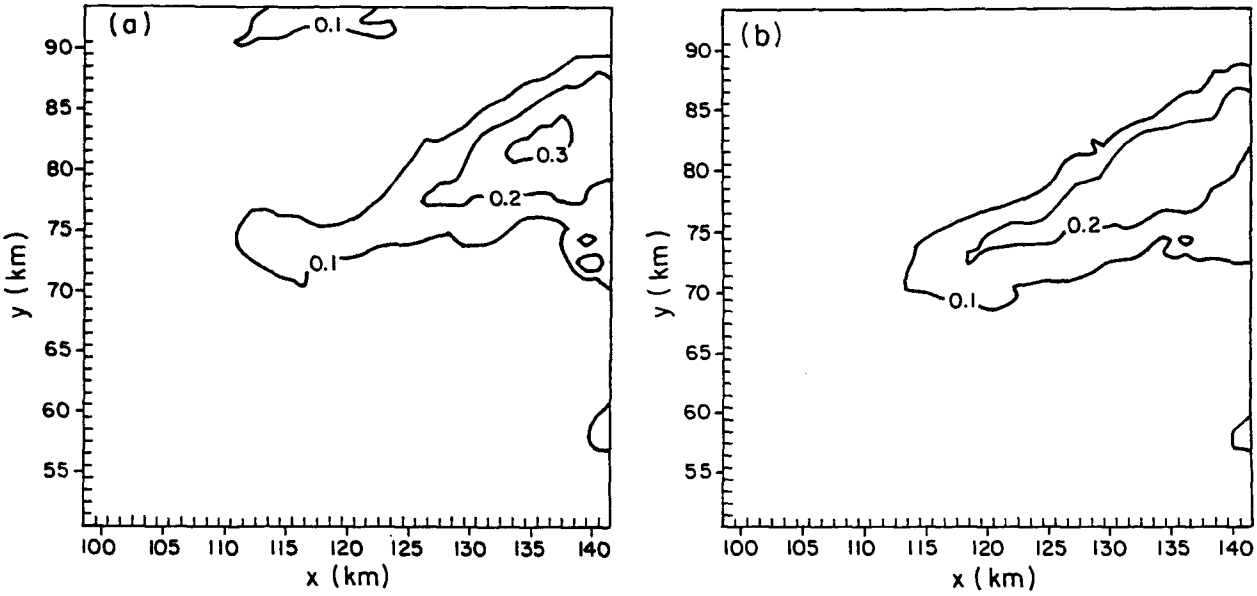

FIG. 9. The simulated pristine ice mixing ratio on grid 3 at 2000 UTC at 3000 m MSL for (a) seeded run and (b) nonseeded run. Contour interval is 0.1 g kg^{-1}.

the peak precipitation rates in the seeded run were 1.0–1.5 mm h^{-1} (not shown).

5. Summary and conclusions

This study has described numerical studies of a seeded orographic precipitation event, with particular detail to implementing explicit ice initiation by artificial ice nucleus aerosols into mesoscale models. In this effort, the results from laboratory studies at CSU (DeMott 1990, 1994) were parameterized, quantifying four ice nucleation mechanisms for the seeding aerosols used in SCPP. Parameterizations were first implemented in a microphysical parcel model compare to DeMott's detailed descriptions of artificial ice formation processes for a representative seeded orographic cloud parcel. Excellent agreement was found. These experiments also indicated that condensation-freezing and deposition nucleation should initially dominate artificial nucleation, with contact-freezing nucleation becoming dominant during parcel ascent and cooling at later times. The contribution of immersion-freezing was deemed insignificant. Earlier papers (DeMott 1991; Deshler and Reynolds 1991) have debated whether or not the contact-freezing mechanism alone could explain ice initiation following seeding of orographic clouds. These new results show that the implementation of more recent laboratory results, including other possible modes of ice formation, does adequately describe ice initiation following seeding. The parcel model simulations also suggested that predicted ice crystal concentrations would be underestimated by a factor of about 3 if one does not account for the change in the aerosol generator PSD during airborne generation. As a consequence of the preliminary calculations, immersion-freezing nucleation was not considered in the mesoscale model simulations, and initial ice nucleus aerosol concentrations and subsequent activation were calculated assuming a PSD characteristic of aircraft generation conditions.

The seeding parameterizations were applied to 3D versions of RAMS that examined the 18 December 1986 SCPP case. This explicit depiction of ice initiation by cloud seeding aerosols represented a unique application for mesoscale models. Three-dimensional simulations of the SCPP case study showed a profound sensitivity to seeding. The model produced good agreement between the simulated natural cloud processes and the observed microphysical structure. The seeded simulation produced large areas with ice crystal concentrations exceeding 20 L^{-1} and peak pristine ice crystal concentrations of 120 L^{-1}, an order of magnitude greater than the ice crystal concentrations produced in the nonseeded run. These simulated concentrations were similar to the observed maximum ice crystal concentrations (100 L^{-1}). Seeding also produced increased pristine ice crystal, aggregate, and graupel mass downstream of the seeded regions in the seeded simulation. Overall precipitation increases due to seeding were 0.1–0.7 mm, similar to values inferred from the observations. Precipitation enhancement in the seeded simulation resulted from increased precipitation efficiency since no marked regions of precipitation deficit occurred due to seeding. These precipitation maxima were collocated with regions of SLW that were enhanced by topographic forcing.

At least two factors for future development of cloud-seeding parameterizations in mesoscale models were identified in this study. First, it was noted that representation of seeding in mesoscale models will probably always be compromised to some extent by the ability to resolve initial concentrations and dispersion of ice nucleus aerosols. Namely, the width of the initial seedline was on a scale much smaller than the very fine resolution (Δx = 1 km) used in this simulation. Subgrid-scale dispersion schemes are needed to address this problem. The ice nucleation schemes used are also very sensitive to small changes in the temperature and humidity, so that subgrid-scale changes in these thermodynamic quantities could also be important.

This study has demonstrated the feasibility for using laboratory results to parameterize the cloud seeding response in an explicit cloud model. These simulations also show promise for a priori evaluations of seeding effects on different cloud types given complete descriptions of ice nuclei behavior. Uncertainties remaining from the standpoint of operational seeding are due to a lack of more complete knowledge of the transient adjustment of temperature and humidity (supersaturation) following combustion, as well as, a lack of better knowledge of particle sizes generated. Resolution of these uncertainties appears quite feasible.

Acknowledgments. Thanks are extended to Drs. David Rogers, Johannes Verlinde, and Robert L. Walko for valuable suggestions. We also appreciate the cooperation of SCPP, the WMO, and other participants of the Third International Modeling Workshop who provided field data and valuable insights on this case. Brenda Thompson helped with the processing of this manuscript. This research was supported by National Science Foundation Grants ATM9118963 and ATM9103748. The lead author would also like to acknowledge the DoD Augmentation Awards for Science and Engineering Research Training under Grant F49620-92-J-0331M and the Air Force Office of Scientific Research under Grant AFOSR-91-0269 for supporting his graduate research.

REFERENCES

Blumenstein, R. R., R. M. Rauber, L. O. Grant, and W. G. Finnegan, 1987: Application of ice nucleation kinetics in orographic clouds. *J. Climate Appl. Meteor.*, **26**, 1363–1376.

Cooper, W. A., 1974: A possible mechanism for contact nucleation. *J. Atmos. Sci.*, **31**, 1832–1837.

Cotton, W. R., M. A. Stephens, T. Nehrkorn, and G. J. Tripoli, 1982: The Colorado State University three-dimensional cloud/me-

soscale model—1982. Part II: An ice phase parameterization. *J. Rech. Atmos.*, **16,** 295–320.

——, G. J. Tripoli, R. M. Rauber, and E. A. Mulvihill, 1986: Numerical simulation of the effects of varying ice crystal nucleation rates and aggregation processes on orographic snowfall. *J. Climate Appl. Meteor.*, **25,** 1658–1680.

DeMott, P. J., 1990: Quantifying ice nucleation by silver iodide aerosols. Ph.D. dissertation, Paper No. 466, Colorado State University, Fort Collins, CO, 253 pp.

——, 1991: Comments on "The persistence of seeding effects in a winter orographic cloud seeded with silver iodide burned in acetone." *J. Appl. Meteor.*, **30,** 1376–1380.

——, 1994: Quantitative descriptions of ice formation mechanisms of silver iodide-type aerosols. *Atmos. Res.*, in press.

——, W. G. Finnegan, and L. O. Grant, 1983: An application of chemical kinetic theory and methodology to characterize the ice nucleating properties of aerosols used in weather modification. *J. Climate Appl. Meteor.*, **22,** 1190–1203.

Deshler, T., and D. W. Reynolds, 1991: Reply. *J. Appl. Meteor.*, **30,** 1381–1384.

——, ——, and A. W. Huggins, 1990: Physical response of winter orographic clouds over the Sierra Nevada to airborne seeding using dry ice or silver iodide. *J. Appl. Meteor.*, **29,** 288–330.

Finnegan, W. G., and R. L. Pitter, 1988: Rapid ice nucleation by acetone-silver iodide generator aerosols. *J. Wea. Mod.*, **20,** 51–53.

Flatau, P. J., G. J. Tripoli, J. Verlinde, and W. R. Cotton, 1989: The CSU-RAMS cloud microphysical module: General theory and code documentation. Atmospheric Science Paper No. 451, Colorado State University, Dept. of Atmospheric Science, Fort Collins, CO, 88 pp.

Gal-Chen, T., and R. C. J. Somerville, 1975a: On the use of a coordinate transformation for the solution of the Navier–Stokes equations. *J. Comput. Phys.*, **17,** 209–228.

——, and ——, 1975b: Numerical solution of the Navier–Stokes equations with topography. *J. Comput. Phys.*, **17,** 276–310.

Hsie, E. Y., R. D. Farley, and H. D. Orville, 1980: Numerical simulation of ice phase convective cloud seeding. *J. Appl. Meteor.*, **19,** 950–977.

Klemp, J. B., and J. Wilhelmson, 1978: The simulation of three-dimensional convective storm dynamics. *J. Atmos. Sci.*, **35,** 1070–1096.

Meyers, M. P., P. J. DeMott, and W. R. Cotton, 1992: New primary ice nucleation parameterizations in an explicit cloud model. *J. Appl. Meteor.*, **31,** 708–721.

Orville, H. D., R. D. Farley, and J. H. Hirsch, 1984: Some surprising results from simulated seeding of stratiform-type clouds. *J. Climate Appl. Meteor.*, **23,** 1585–1600.

Plooster, M. N., and N. Fukuta, 1975: A numerical model of precipitation from seeded and unseeded cold orographic clouds. *J. Appl. Meteor.*, **14,** 859–867.

Rauber, R. M., 1981: Microphysical processes in two stably stratified orographic cloud systems. Atmospheric Science Paper No. 337, Colorado State University, Fort Collins, CO, 151 pp.

Reynolds, D. W., and A. S. Dennis, 1986: A review of the Sierra Cooperative Pilot Project. *Bull. Amer. Meteor. Soc.*, **67,** 513–523.

——, and A. P. Kuciauskas, 1988: Remote and in situ observations of Sierra Nevada winter mountain clouds: Relationship between mesoscale structure, precipitation, and liquid water. *J. Appl. Meteor.*, **27,** 140–156.

Rogers, D. C., P. J. DeMott, and L. O. Grant, 1994: Concerning primary ice nuclei concentrations and water supersaturations in the atmosphere. *Atmos. Res.*, **33,** 151–168.

Rokicki, M. L., and K. C. Young, 1978: The initiation of precipitation in updrafts. *J. Appl. Meteor.*, **17,** 745–754.

Stith, J. L., D. Burrows, and P. J. DeMott, 1994: Initiation of ice: Comparison of numerical model results with observations of ice development in a cumulus cloud. *Atmos. Res.*, **32,** 13–30.

Tripoli, G. J., and W. R. Cotton, 1981: The use of ice–liquid water potential temperature as a thermodynamic variable in deep atmospheric models. *Mon. Wea. Rev.*, **109,** 1094–1102.

——, and ——, 1982: The Colorado State University three-dimensional cloud/mesoscale model—1982. Part I: General theoretical framework and sensitivity experiments. *J. Rech. Atmos.*, **16,** 185–220.

——, and ——, 1989: Numerical study of an observed orogenic mesoscale convective system. Part I: Simulated genesis and comparisons with observations. *Mon. Wea. Rev.*, **117,** 273–304.

World Meteorological Organization, 1994: Report of the Third International Cloud Modeling Workshop. WMP Rep. No. 20.

Young, K. C., 1974a: The role of contact nucleation in ice phase initiation in clouds. *J. Atmos. Sci.*, **31,** 768–776.

——, 1974b: A numerical simulation of wintertime orographic precipitation: Part I. Description of model microphysics and numerical techniques. *J. Atmos. Sci.*, **31,** 965–973.